ANL-82-68

ARGONNE NATIONAL LABORATORY
9700 South Cass Avenue
Argonne, Illinois 60439

ADVANCED FUEL-CELL DEVELOPMENT

Progress Report for
October—December 1981

by

R. D. Pierce, R. M. Arons,* J. T. Dusek,*
A. V. Fraioli, G. H. Kucera, J. W. Sim,
J. L. Smith, and J. R. Stapay

Chemical Engineering Division

April 1983

TABLE OF CONTENTS

LIST OF FIGURES

LIST OF TABLES

ADVANCED FUEL CELL DEVELOPMENT

Progress Report for
October-December 1981

by

R. D. Pierce, R. M. Arons,* J. T. Dusek,* A. V. Fraioli,
G. H. Kucera, J. W. Sim, J. L. Smith, and J. R. Stapay

ABSTRACT

This report describes fuel cell research and development
activities at Argonne National Laboratory (ANL) during the period
October through December 1981. These efforts have been directed
toward (1) improving understanding of component behavior in molten
carbonate fuel cells and (2) developing alternative materials and
concepts for components. The principal focus was changed during
this period from the development of cathodes fabricated from NiO
and electrolyte supports of sintered γ-LiAlO$_2$ to an investigation
of NiO cathode dissolution and deposition and a search for alterna-
tive cathode materials.

SUMMARY

Electrolyte Development

A large batch of slip was prepared for casting tapes (13 by 13 cm) con-
taining β-LiAlO$_2$. These tapes will be sintered and impregnated with carbon-
ates for cell testing.

Results are presented for sessile drop measurements (made during 1976)
of the wetting of nickel, 316 SS, gold, and LiAlO$_2$-coated Al$_2$O$_3$ surfaces by
Li$_2$CO$_3$-K$_2$CO$_3$ mixtures prepared from reagent-grade carbonates. Under a cathode
gas, a zero contact angle was observed with all of these materials as soon as
the salt wetted. Under an anode gas, contact angles ranging from 30 to 130°
were observed for the salt on the nickel and gold surfaces, and several minutes
were required before constant angles occurred. When high-purity Li$_2$CO$_3$ was
used to prepare the salt, complete wetting was observed with each of the metals
after a brief induction period. Apparently some impurity in reagent-grade
Li$_2$CO$_3$ decreases the wetting of the metals by Li$_2$CO$_3$-K$_2$CO$_3$ under a reducing
atmosphere.

Cathode Development

Sintered NiO

Organic pore formers are being investigated to increase the coarse poros-
ity of sintered NiO structures. Fibers are attractive because they reinforce

_____
*Materials Science Division, ANL.

the green body before firing, as well as introduce connected porosity. Most of the work has been done with 2-μm dia by 3-mm long nylon fibers. Homogeneous mixing of fibers and NiO was obtained in a plastic mix using a sigma-blade mixer.

Starch, in concentrations up to 15 wt %, also has been promising as a pore former and may be useful in combination with fibers.

NiO Solubility

Preparations are being made to measure the solubility of NiO and other potential cathode materials in molten $Li_2CO_3-K_2CO_3$. A technique that entails absorbing the equilibrated liquid into porous disks is being considered.

Alternative Cathode Materials

Cathode materials must have adequate electronic conductivity and chemical stability. Ideally, the material should be stable at both electrodes so that source-sink diffusional processes such as occur with NiO are avoided. For example, the Zn^{2+} which would be in equilibrium with a ZnO cathode would not be reduced under anode conditions. We plan to study materials like ZnO that do not reduce in the anode environment.

Preliminary fabrication tests were made by cold pressing ZnO with a paraffin binder. The ZnO samples were prepared both with and without 2-1/2 wt % Al_2O_3 dopant. The samples were sintered at 1000°C in air for 2 h. The Al_2O_3 completely changed the ZnO particles and lowered the resistivity by a factor of 100. A sample treated with LiOH and heated in air had very high resistivity. The Al_2O_3 should enhance and Li_2O should poison the n-type semiconductivity of ZnO. No further work is planned on ZnO at this time.

Cell Testing

A preliminary cell test (SQ-30) involving a cathode fabricated from sintered NiO powders was completed after about 500 h. For this cathode, the desired dual pore sizes were obtained by sintering ~40-μm-dia agglomerates containing fine pores (<1 μm). Although the cell performance was lower than standard ANL tests, the difference was less than expected. Much of the cathode area internal to the agglomerates is believed to be inactive. We are attempting to eliminate the need for large agglomerates by incorporating pore formers in future cathodes.

Two cells (SQ-31 and SQ-33) were run to study cathode dissolution and deposition in the tile. To increase the solubility of nickel at the cathode, the operating temperature for this cell was increased from 650 to 700°C, and the CO_2 concentration was increased from 30% to 95%. Cell SQ-31 was shut down after 240 h but has not been examined. Cell SQ-33 is still in operation.

Cell SQ-32 was operated to duplicate cell test SQ-25, in which a thin layer of partially reduced $NiAl_2O_4$ was placed between the cathode and tile. As was the case for SQ-25, the performance of cell SQ-32 reached its steady-state level in about 50 h rather than the more typical 150 h. The possibility that infusion of corrosion products is involved in the initial increase in performance is being considered.

Posttest Evaluations

Posttest examination of cell LR-2 was completed. This cell was run for 2400 h to study cathode potential relaxation following current interruption. The surface area of the $LiAlO_2$ in the posttest tile was 15 m^2/g, which reflects the typical surface area loss found in earlier posttest tiles.

A number of analytical techniques were considered for determining the nickel content of used tiles. Two analytical approaches are being used: (1) semiquantitative profiling of pieces of tile to assess nickel distribution and identify species and (2) a quantitative chemical determination of total nickel content. Four tiles were analyzed, and the results indicate comparable nickel transfer rates from the cathode. The rates project total dissolution of the cathode in about 1.2 x 10^4 h.

Microscopic examinations were conducted with both electron and light microscopes. Nickel precipitates were observed. Most of these are metallic, but some nonmetallic precipitates, probably $LiNiO_2$, also were noted. Original identification of the phases was made with scanning electron microscopy (SEM) techniques, and then low-power ($\sim$100 X) light microscopy was employed for scanning and assessing samples. Polarization is useful for enhancing optical contrasts.

I. INTRODUCTION

The advanced fuel cell studies at Argonne National Laboratory (ANL) are part of the DOE Advanced Fuel Cell Program. The objective of this DOE program is to reduce the technical uncertainties with fuel cells so that manufacturers and users can introduce high-efficiency generating systems, which have the capability of operating on coal or other fuels. At the present stage of development, the primary thrust of the ANL program is to provide supporting research and development that pursues fundamental understanding of fuel cell behavior and investigates alternative stack concepts.

The present molten carbonate fuel cells consist of a porous nickel anode, a porous lithiated nickel oxide cathode, an electrolyte structure which separates the anode and cathode and conducts only ionic current between them, and appropriate metal housings or, in the case of stacks of cells, intercell separator sheets. The cell housings (or separator sheets) bear upon the electrolyte structure to form a seal between the environment and the anode and cathode gas compartments. The usual electrolyte structure, which is commonly called "tile," is a composite of discrete $LiAlO_2$ particles and a mixture of alkali metal carbonates. The carbonates are liquid at the cell operating temperature of about 925 K. At the anode, hydrogen and carbon monoxide in the fuel gas react with carbonate ion from the electrolyte to form water and carbon dioxide while giving up electrons to the external circuit. At the cathode, carbon dioxide and oxygen react and accept electrons from the external circuit to re-form carbonate ion, which is conducted through the electrolyte to the anode. In a practical cell stack, CO_2 for the cathode probably would be obtained from the anode exhaust.

The ANL contribution to the program is intended to provide understanding of cell behavior and to develop improved components and processes. Improvements are needed most in the cathode and electrolyte structure, which are receiving special attention at ANL.

Electrolyte structures employing a sintered $LiAlO_2$ matrix are being examined as an alternative to tiles, which are a paste-like mixture of fine $LiAlO_2$ particles and carbonate salt. Characterization of electrolyte-structure properties and the relation of the properties to cell behavior are of major importance. Determination of the stability of the structure is also of high priority.

Until recently, general practice involved assembling cells with a sintered nickel cathode, which reacts in situ with the oxidant gas and the electrolyte to form lithiated nickel oxide. The "lithiation" is important to give the cathode adequate electronic conductivity. At ANL nickel oxide cathodes for assembly in cells have been developed to improve cell performance through better conductivity, strength, and dimensional stability of the cathode. With these cathodes, lithiation may be performed in-cell or out-of-cell, but generally is performed in-cell. However, recent observations of nickel dissolution from the cathode followed by deposition of metallic nickel in the electrolyte raises doubt about the suitability of NiO cathodes for long-lived cells. Study of the nickel dissolution problem and evaluation of possible alternative cathode materials are our principal current activities.

Cells are operated to assess the behavior of the electrolyte and other components and to understand the performance of life-limiting mechanisms at work within the cell. Cell operation is coupled with efforts on diagnostics and materials development.

II. ELECTROLYTE DEVELOPMENT

A. Fabrication of Sintered Structures via Tape Casting
(J. W. Sim)

A large batch of slip is being prepared for casting tapes (~13 by 13 cm) containing β-LiAlO$_2$. These tapes will be sintered and impregnated with carbonates, with the objective of producing a structure suitable for cell testing, i.e., a structure containing no gross cracks. Previous experiments (ANL-82-67, p. 5) with smaller (~5 by 5 cm) structures indicated that about half of them had no gross cracks. If cracking is more severe for the larger structures, development of sintered LiAlO$_2$ electrolyte structures may be discontinued.

B. Wetting Behavior of Carbonate Electrolytes
(G. H. Kucera[*])

During August-December 1976, J. G. Eberhart conducted a study of the wetting behavior of molten carbonate electrolyte on various substrates. The effect on electrolyte wetting of temperature, electrolyte composition, salt purity, and gaseous environment also was investigated. The following is a summary of that study, along with Eberhart's recommendations for other cell-related studies.

The substrates were commercial-grade nickel-200 (99% pure), MARZ-grade nickel (99.995% pure), gold, 316 stainless steel, and LiAlO$_2$-coated Al$_2$O$_3$. Where appropriate, the temperature was varied from about 775 to 975 K. The electrolyte mixtures consisted of Li$_2$CO$_3$ and K$_2$CO$_3$. Three salt compositions were used: lithium-rich eutectic (38 mol % K$_2$CO$_3$), equimolar compound (50 mol % K$_2$CO$_3$), and potassium-rich eutectic (57.3 mol % K$_2$CO$_3$). Each composition was prepared from either ultra-pure (Li$_2$CO$_3$ purity = 99.97%) or reagent-grade compounds (purity about 99%). The gaseous environment consisted of either an anode or cathode gas. Contact angle measurements were made with an optical goniometer on specimens that were contained in a test assembly equipped to accommodate evacuation and changes in gas composition.

The contact angle measurements in a static cathode gas environment (67% CO$_2$, 33% O$_2$) showed little or no dependence on substrate (the surface of the nickel substrate was now oxidized), temperature, electrolyte composition, or purity. In all cases, the salt spread immediately upon melting, indicating a contact angle, θ, of 0°.

The electrolyte wetting behavior on these same substrates in a static anode gas environment (80% H$_2$, 20% CO$_2$) was significantly different. When the electrolyte mixtures were prepared from ultra-pure Li$_2$CO$_3$ and K$_2$CO$_3$, a sessile drop formed at about the melting temperature of the mixture on the nickel (200 and MARZ grade), 316 SS, and LiAlO$_2$ surfaces. Initially, the drop had nonzero advancing, θ_A, and receding, θ_R, contact angles; after a few minutes, however, the drop spread over the entire substrate.

In the anode gas environment, electrolyte mixtures prepared from reagent-grade salts exhibited different melting and wetting behavior from that of mixtures prepared from ultra-pure salts. These reagent-grade mixtures did not melt quickly but melted gradually over a wide temperature range that varied from 50 to 200°. The sessile drop observed over this temperature range appeared to have dendritic growths and gas bubbles near the liquid-vapor interface. In addition, a solid-like skin formed on the drop at this same interface. The skin disappeared when the temperature reached about 975 K and the drop then assumed the classical shape. Contact angles measured after this time, for the temperature range 825 to 975 K, are $\theta_A = 132 \pm 4°$ and $\theta_R = 53 \pm 8°$ for the lithium-rich eutectic on the MARZ-grade nickel substrate; $\theta_A = 81 \pm 5°$ and $\theta_R = 32 \pm 3°$ for the equimolar compound on the nickel-200 substrate; and $\theta_A = 73 \pm 2°$ and $\theta_R = 50 \pm 4°$ for the equimolar compound on the gold substrate. Although the wetting behavior of these two electrolytes on the nickel and gold substrates is independent of temperature, considerable time (up to 60 min) was required before a constant contact angle was achieved.

After the measurements were completed for the equimolar electrolyte on the nickel-200 substrate, the test assembly was cooled to room temperature and evacuated, and its gaseous environment was changed to the cathode gas. About 1-2 min after reaching the melting temperature of the mixture, the electrolyte spread on the substrate. This finding suggests that the reagent-grade electrolytes contained one or more impurities that have no observable effect in the cathode gas environment. Two additional experiments were conducted to determine which reagent-grade salt was responsible for the poor electrolyte wetting behavior in the anode gas. In the first, the electrolyte consisted of 62 mol % ultra-pure Li_2CO_3 and 38 mol % reagent-grade K_2CO_3. After melting, a sessile drop initially formed on a MARZ-nickel substrate, with θ_A of about 70-90°; however, after about five minutes, the drop spread over the substrate. In the second experiment, the electrolyte consisted of 62 mol % reagent-grade Li_2CO_3 and 38 mol % ultra-pure K_2CO_3. The equilibrium measurement showed θ_A to be about 44° and θ_R to be about 22° on a MARZ-nickel substrate.

Due to time constraints, the impurity responsible for the poorer wetting behavior of electrolytes containing reagent-grade Li_2CO_3 was not identified nor was the wetting behavior of the electrolytes on a chromium-stabilized nickel substrate investigated. The importance of these issues to actual fuel cells is apparent. In addition, it might be of interest to determine (1) the effect of impurity level on the molten-salt wetting and (2) the effect of chromium content on the wettability of nickel-chromium alloys by the molten carbonates.

Another aspect of molten carbonate wetting that is relevant to fuel cell operation is the electrocapillarity effect. When an electrical potential is applied across a solid-liquid interface, not only is the double layer structure of the interface affected but also the interfacial tension is altered. Measurement of the contact angles at different applied potentials is relatively easy and has been attempted for fused-salt systems.[1] Such a study could be carried out for reagent-grade carbonates in the anode environment after the impurities in the salts have been characterized.

III. CATHODE DEVELOPMENT

A. Development of Sintered NiO Cathodes—Use of Pore Formers
    (R. M. Arons and J. T. Dusek)[*]

We have begun experiments on incorporation of organic fibers and powders into a NiO green body. These organics are intended to serve a two-fold purpose. First, the organic materials will burn out upon firing, leaving behind voids or pore channels in the sintered pieces. Second, for the case of fibers, they serve to reinforce the green body and provide the greater handling strength especially required for thin cathode plates. The natural problems one encounters in filling a body with fibers are (1) the homogeneous dispersal and deflocculation of the fibers and (2) incorporation of a high enough volume fraction of fiber into the body.

Currently, we have procured fibers of cotton, nylon, rayon, polyester, sisal, and manila hemp. The preponderance of our work has been done with the nylon fibers, which are 20-μm dia by 3-mm long. We are awaiting delivery of graphite fibers in two sizes: 3-5 mm long by 12.5-20 μm dia and 6 mm long by 14 μm dia.

Our first set of experiments was to incorporate various fibers into our standard body of cold-pressed agglomerates. Dispersal of fibers was difficult in a dry-mixing operation, and no real improvement in the sintered microstructure was evident. Moreover, it was difficult to distinguish pore channels due to volatilized fibers from porosity between packed agglomerates.

In the second phase of our work, we incorporated pore formers into experimental batches of as-received (nonagglomerated) NiO and Li_2CO_3 powders.

A plastic mix, denoted NF-5 and described in Table 1, was prepared in a "sigma blade" mixer, which allows a homogeneous dispersal of fibers throughout the mix and minimizes the clumping together of two or more fibers into floccules. This type of mix has the consistency of modeling clay and can readily be worked into the desired shape without segregation of its constituents. Mix NF-5 was extruded into a rod shape through a 1/2-in. dia circular die. The rod was then flattened with a rolling pin into 1-1/4 mm thick sheet and finally was fired in air for 1 h at 1100°C. The final fired plates are 75.6% dense.[†] This relatively high density is due to the low volume fraction of pore formers and the high degree of working.

A second batch, denoted NF-6, was made similarly to NF-5 except that it was 20% larger and contained 13.4 g of nylon fibers. This batch was not extruded prior to being flattened by hand with a rolling pin. A sheet of NF-6 was fired at 1050°C for 1/2 h and was found to be 61.9% dense. We feel that the nylon content was low and could be increased significantly without causing other problems.

---

[*]Materials Science Division, ANL.

[†]All NiO densities in this report are based on the theoretical density of pure NiO of 6.808 g/cm^3.

Table 1. Batch Content of Mix NF-5

1000 g	NiO
25 g	Li_2CO_3
20 g	Ammonium alginate
10 g	Methocel
6.1 g	Nylon fiber
175 g	H_2O
14 cc	Mobilcer "C" wax

A second series of experiments was done using cornstarch as a pore former. Mixtures of NiO and Li_2CO_3 were made up with varying percentages of powdered cornstarch, ranging from 0 to 40% by weight as given in Table 2. Each of these mixes was cold pressed at 1000 lb_F in a 1-1/4 in. dia die (∿5.6 MPa) and then fired for 1/2 h at 1050°C. Starch contents of 20% or greater were too large, resulting in bodies which are difficult to handle because of high friability. Lesser starch contents resulted in attractive microstructures and usefully high pore volumes, e.g., 55% porosity with 15% starch and 49% porosity with only 10% starch. A starch-type pore former is expected to be useful either by itself or in some combination with fibrous pore formers or with the standard agglomerate technique.

A final experiment was conducted with a plastic mix, denoted NF-7 and made by mixing ∿10% starch and some additional water to the remainder of batch NF-6. A piece of this mix was rolled to about 1.6 mm thickness and fired for 1/2 h at 1050°C. This plate fired to a density of 47-50% of theoretical. Even at this density, the piece has a surprisingly good handling strength. Again, as in NF-6, considerably more nylon would be required to optimize the micro-structure.

B. **Nickel Oxide Solubility in Molten Carbonates**
     (J. W. Sim)

Preparations are being made to measure the solubility of NiO and other potential cathode materials in molten Li_2CO_3 (62 mol %)-K_2CO_3 (38 mol %). Samples of NiO (or other potential cathode materials) will be allowed to equilibrate with the carbonates, and then aliquots of the liquid carbonates will be removed for analysis.

One technique being considered for sampling involves dipping porous sintered $LiAlO_2$ discs into the carbonates, and then withdrawing the discs after they have absorbed the carbonates. Two discs are used for each sampling. The bottom disc contacts the carbonate melt, while the top disc remains above the melt but absorbs carbonate from the lower disc. The purpose of this

Table 2. Results of Experiments with Lithiated NiO Cold Pressed
with Cornstarch

Normal Starch Content, %	Wt. NiO, g	Wt. Starch, g	Wt. Li$_2$CO$_3$, g	Porosity, %	Comments
40	3.0	2.0	0.125	a	Not handleable
30	3.5	1.5		a	Not handleable
20	4.0	1.0		65	Weak
15	4.25	0.75		55	Handleable
10	4.5	0.5		49	
5	4.75	0.25		38	
0	5 0	0		29	

^{a}None available.

procedure is to prevent the sampling of NiO particles, which may be suspended in the melt. The bottom disc, therefore, acts as a filter and is not analyzed. The top disc is be dissolved in acid and analyzed.

The analysis of the carbonate samples, after they are obtained, was discussed with K. J. Jensen of ANL's Analytical Chemistry Laboratory. For nickel, if it is present in the concentrations found by General Electric Co. (about six micrograms per gram of carbonates), either of two techniques for chemical analysis can be used--flame atomic absorption of the dissolved sample or a spectrophotometric measurement on the dissolved sample. The estimated error for the former procedure is about 3-5% (at this level of nickel), and the estimated error for the latter procedure is about 1%. The presence of large amounts of dissolved aluminum (from LiAlO$_2$) may cause problems in flame atomic absorption, while the presence of undissolved material will interfere with the spectrophotometric determination. If nickel is present at significantly lower concentration than that found by General Electric, the relative error in either analytical procedure will increase, and furnace atomic absorption may be required for the analysis. No matter which analytical procedure is used, some development work will be required in order to ensure that the analytical results are accurate. Also, for lower nickel concentrations in the melt, further refinement will be required in the analytical procedures.

C. Alternative Cathode Materials--Nonreducible Cathodes
(J. W. Sim)

Using the data compiled by Ingram and Janz,[2] we have developed an emf series that is helpful in understanding the problem of NiO dissolution and subsequent deposition in the electrolyte tile (or at the anode). In this series, the electrical potentials for a variety of equilibria (and reactant concentrations) are determined. Then, by comparing these potentials to the

expected anode potentials, one can determine whether a given reaction is likely to occur in the anode environment. Using this analysis, it was discovered that certain materials dissolve in the cathode environment but do not deposit in metallic form in the anode environment. Such materials are candidates for alternative cathode materials.

The emf series discussed above is given in Table 3. For the purpose of this discussion, the potential of the cathode reaction:

$$CO_2 + 1/2\ O_2 + 2e^- \rightarrow CO_3^{2-} \tag{1}$$
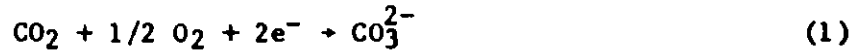
was defined as 0.000 V for $pCO_2 = 0.67$ atm and $pO_2 = 0.33$ atm. For a typical cathode gas composition ($\sim 30\%\ CO_2$, 70% air), the potential would be -0.045 V at open circuit. For the reverse anode reaction:

$$H_2O + CO_2 + 2e^- \rightarrow CO_3^{2-} + H_2 \tag{2}$$
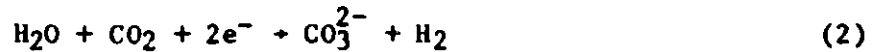
the potential would be -1.120 V at open circuit (for ANL standard fuel 78% H_2-19% CO_2-3% H_2O). Under load, the potential in the anode environment might approach -0.970 V. For leaner fuels, the anode potential range would be somewhat less negative.

For the equilibria in Table 3, the rule of thumb is: the product of any given reaction will be oxidized by the reactants of any other reaction whose electrode potential is more positive. Thus, all of the reactions having potentials between 0 and -1.120 V can occur in the anode of a cell at open circuit (or between 0 V and approximately -0.970 V, under load). For example, the reduction of Ni^{2+} to nickel metal (potential = -0.84 V) will occur in the anode environment when the melt is saturated with Ni^{2+} from NiO dissolution at the cathode. Conversely, any reaction having a potential more negative than -1.120 V cannot occur in the anode environment. For example, zinc metal will not form in the anode environment (potential = -1.35 V) when the Zn^{2+} concentration in the melt is the amount expected from ZnO dissolution at the cathode. If zinc ions cannot be reduced from a saturated melt, dissolution of ZnO will proceed only until the melt is saturated with Zn^{2+}.[*] As a result, consumption of the cathode via dissolution is negligible, and the creation of short circuits via metal deposition is not possible. We plan to study materials like ZnO, which are not reduced in the anode environment.

D.   Alternative Cathode Materials
      (J. L. Smith, J. W. Sim, and A. V. Fraioli)

Some preliminary tests were done on cathode alternatives to NiO. In particular, several structures were fabricated from ZnO, which was chosen because it is one of many possible nonreducible cathode materials and has been previously used in a molten carbonate fuel cell environment.[3,4]

---

[*]Note: If the solubility of Zn^{2+} within the tile decreases because of a local CO_2 activity lower than that at the cathode, ZnO may precipitate and promote zinc mass transport from the cathode.

Table 3. Electrode Potentials in Molten Carbonates at 600°C[a]

Electrode Potential, V	Electrode Reaction	Conditions
0.000 (defined)	$CO_2 + 1/2 \; O_2 + 2e^- \rightarrow CO_3^{2-}$	$pCO_2 = 0.67$ atm, $pO_2 = 0.33$ atm
-0.045	$CO_2 + 1/2 \; O_2 + 2e^- \rightarrow CO_3^{2-}$	$pCO_2 = 0.30$ atm, $pO_2 = 0.15$ atm $pN_2 = 0.55$ atm ($\sim$30% CO_2, 70% air)
-0.34	$Ni^{2+} + 2e^- \rightarrow Ni$	$[Ni^{2+}] = 1$ mole fraction
-0.39	$Co^{2+} + 2e^- \rightarrow Co$	$[Co^{2+}] = 1$ mole fraction
-0.66	$Fe^{2+} + 2e^- \rightarrow Fe$	$[Fe^{2+}] = 1$ mole fraction
-0.84	$Ni^{2+} + 2e^- \rightarrow Ni$	$[Ni^{2+}] = 1.7 \times 10^{-6}$ mole fraction (saturated melt for cathode gas with $pCO_2 = 0.30$ atm)
-0.89	$Zn^{2+} + 2e^- \rightarrow Zn$	$[Zn^{2+}] = 1$ mole fraction
-0.91	$Co^{2+} + 2e^- \rightarrow Co$	$[Co^{2+}] = 9.1 \times 10^{-7}$ mole fraction (saturated melt for cathode gas with $pCO_2 = 0.30$ atm)
-1.08	$Fe^{2+} + 2e^- \rightarrow Fe$	$[Fe^{2+}] = 1.4 \times 10^{-5}$ mole fraction (saturated melt for cathode gas with $pCO_2 = 0.30$ atm)
-1.12	$H_2O + CO_2 + 2e^- \rightarrow H_2 + CO_3^{2-}$	$pH_2 = 0.526$ atm, $pH_2O = 0.250$ atm, $pCO_2 = 0.083$ atm (ANL standard fuel)
-1.35	$Zn^{2+} + 2e^- \rightarrow Zn$	$[Zn^{2+}] = 4.9 \times 10^{-6}$ mole fraction (saturated melt for cathode gas with $pCO_2 = 0.30$ atm)
-1.38	$Mn^{2+} + 2e^- \rightarrow Mn$	$[Mn^{2+}] = 1$ mole fraction
-1.67	$Mn^{2+} + 2e^- \rightarrow Mn$	$[Mn^{2+}] = 4.0 \times 10^{-4}$ mole fraction (saturated melt for cathode gas with $pCO_2 = 0.30$ atm)

[a]Developed from data in Ref. 2.

Samples were made by cold pressing ZnO powder with paraffin binder. Samples also were prepared with nylon fibers and with 0.5 wt % Degussa alumina added to the ZnO and binder. All samples were sintered at 1000°C in air for two hours and, in all cases, the sintered body was found to be strong and handleable. Scanning electron microscopy (SEM) revealed that the nylon fibers produced well-defined tubular passages of the fiber diameter (15-20 μm) through the sintered structure of ZnO particles ($\sim$1 μm dia). The inclusion of 2-1/2 wt % Degussa Al_2O_3 resulted in a complete change of the ZnO particulate appearance to a platelet-like structure.

The inclusion of Al_2O_3, Cr_2O_3, or Ga_2O_3 in ZnO should enhance the n-type semiconductivity.[3,4] The ZnO sample with alumina contained the amount necessary to optimize conductivity according to Ref. 4. A sample also was saturated with LiOH and heated in air to examine the influence of lithium content on conductivity.

Preliminary resistivity measurements were made on ZnO pellets pressed from powders with and without alumina dopant. The resistivities were high and erratic and showed polarization effects with dc, four-point probe techniques. For the pure ZnO, the resistivities ranged from 10^5 $\Omega \cdot cm$ at 200°C to 10^3 $\Omega \cdot cm$ at 1000°C; with the included alumina, the resistivities were lower and ranged from 10^3 $\Omega \cdot cm$ at 200°C to 10 $\Omega \cdot cm$ at 1000°C. The sample treated with LiOH exhibited immeasurably small dc conductivity up to 700°C. These resistivity values do not agree well with some published values.[4] Preparation procedures are often critical and may affect conductivity by several orders of magnitude. Further work on ZnO will await an assessment of other candidate materials.

IV. CELL TESTING

A. Cell Operation
(J. L. Smith, J. W. Sim, A. V. Fraioli, and J. R. Stapay)

During this quarter, testing of cells SQ-30 to SQ-37 was completed. Cell SQ-33, assembled to examine cathode dissolution and deposition, is still under test after about 1200 h.

Testing of cell SQ-30 was terminated after about 488 h. The purpose of this cell was to test a cathode fabricated by agglomerating fine (<1 μm) NiO particles with binder and Li_2CO_3. This mixture was dried, crushed, and sieved to give ∼40-50 μm-dia agglomerates of the submicron-sized NiO particles. These agglomerates were then cold pressed into a plate and sintered at 1000°C for 1 h. The result is a microstructure consisting of packed, sphere-like agglomerates of submicron-sized NiO particles. The cathode thickness was 0.61 mm, with a total variation of less than 0.10 mm. The characteristics of the remaining components were nominally identical to those of the components normally used.

As previously reported (ANL-82-67, p. 19), cell SQ-29 had low cross-leakage of hydrogen from the anode to the cathode (2.3 x 10^{-5} to 4.0 x 10^{-5} mol/min). It was proposed that the low level of cross-leakage resulted from the use of a new batch of $LiAlO_2$/carbonate powder in the tile, because no diffusion barrier was incorporated in cell SQ-29. The tile in cell SQ-30 was pressed from the same batch of powder, and the level of cross-leakage was 5.8 x 10^{-5} mol/min. This low level indicates that the new batch of powder produces tiles that are more impervious to cross-leakage.

The electrochemical performance of cell SQ-30 was lower than that typical of ANL cells (Fig. 1). Moreover, SQ-30 was slow (200 h) in attaining its maximum performance (0.83 V at 80 mA/cm^2) and exhibited unusual behavior after being run under load. After steady performance had been attained (215 h), the cell was run under load for six hours. After this period, there was a significant improvement in performance (gain of 21 mV at 80 mA/cm^2, anode and cathode utilization of 75%). This test was repeated at about 300 h, with a gain in voltage of 14 mV. Although the performance of this cell was lower than that of the standard ANL cell, the difference was less than might be expected from the first test of such a drastically different cathode microstructure (as compared to the preoxidized cathodes).

During operation of cell SQ-30, the anode compartment was purged continually with fuel. This purging is a departure from our standard operating procedure, where fuel flow for the anode is replaced by helium for various periods of time during startup, termination, and leakage testing. This change in procedure was used because cell SQ-29, in which only a few brief tests with helium on the anode were performed at the end of cell operation, had practically no cathode corrosion products deeply infused into the tile. Posttest examination of the tile in cell SQ-30 indicated, once again, shallow cathode corrosion product infusion. This finding suggests that the absence of hydrogen during the use of helium in the anode and/or the new batch of the material used for these tests had a direct effect on the infusion process.
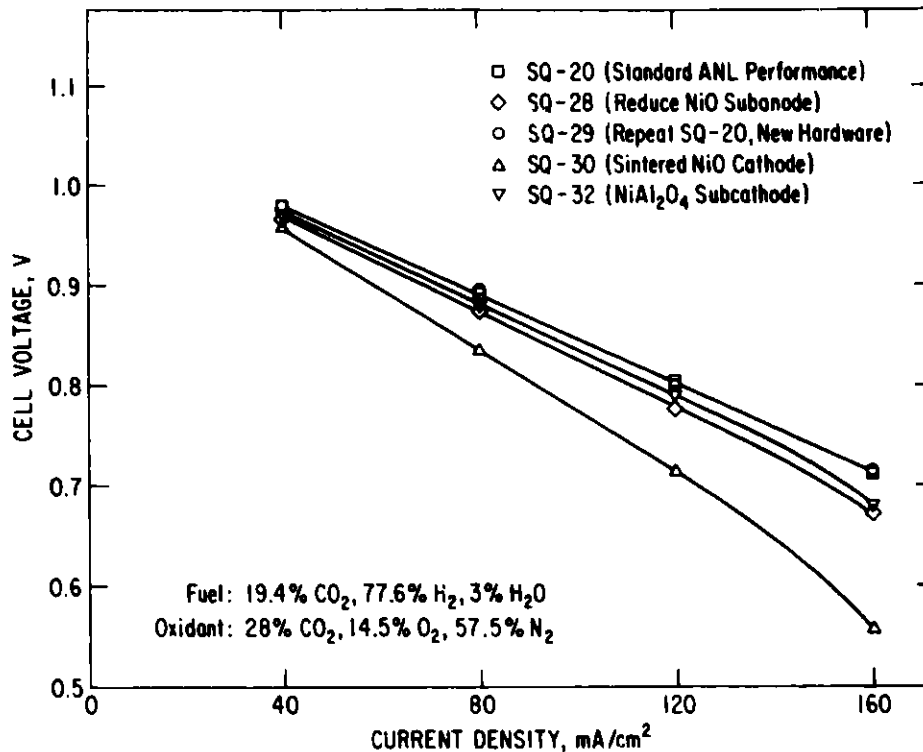
Fig. 1. Constant Flow Polarization Data for Cells SQ-20,
-28, -29, -30, and -32 (75% fuel utilization
and 25% oxidant utilization at 160 mA/cm²)

The objective of cells SQ-31 and SQ-33 is to study cathode dissolution and deposition in the tile. The postulated dissolution-deposition mechanism is as follow: an equilibrium is established between NiO, CO_2, and $NiCO_3$ (a soluble species); nickel ion diffuses across the cell, driven by a concentration gradient; and then hydrogen, which diffuses into the tile from the anode side, reacts within the tile to reduce the nickel ion, thereby creating the concentration gradient. The dissolution-deposition rate will be enhanced by increased CO_2 partial pressure at the cathode and by increased temperature, both of which increase the nickel ion concentration in a saturated melt.

Cell SQ-31 was run at 700°C, with high CO_2 content gas (95% CO_2, 5% O_2) on the cathode side and lean fuel (34% H_2, 24% CO_2, 42% N_2) on the anode side. The tile was thinner than usual (∿1.17 mm vs. 1.9 mm) to shorten the diffusion path and, hence, increase the nickel deposition rate. Five grams of electrolyte eutectic, an amount just below that which the electrodes should take up during cell operation, was added at the anode-tile interface during cell assembly. The fully wet tile and electrodes should allow a maximum nickel migration rate. This cell was shut down at approximately 240 h because of severe cross-leakage. Based on cell test results of United Technologies Corp., this time should be sufficient to deposit a significant amount of nickel within the tile. No analysis for nickel in the tile has been done yet.

Cell SQ-33 is a replacement for SQ-31. It is identical to SQ-31 except that 5 g of eutectic was melted into the anode prior to cell assembly. It is being run on standard fuel (78% H_2-19% CO_2-3% H_2O) rather than lean fuel. The cell currently has run approximately 1200 h and is operating normally.

Cell SQ-32 was an attempt to duplicate the construction and performance of SQ-25 (ANL-82-40, p. 14), in which a layer of partially reduced nickel aluminate was incorporated as a subcathode in the cell assembly. To this end, ~0.9 g of nickel aluminate was spray-coated onto a preoxidized nickel-plaque cathode, and the cell was tested, with particular attention being given to the acquisition of constant-flow polarization data as a function of time. These data are normally acquired once near the end of a test after the cell voltage has stabilized. Figure 2 presents the cell voltage exhibited during many recent cell tests. As shown, the performance of cell SQ-32 duplicated the rapid rise to the plateau voltage of SQ-25. The final constant-flow polarization data for SQ-32 and the standard ANL cell (no barrier layer) are shown in Fig. 1. The deviation from nonlinear behavior is attributed to diffusion limitations at higher currents.
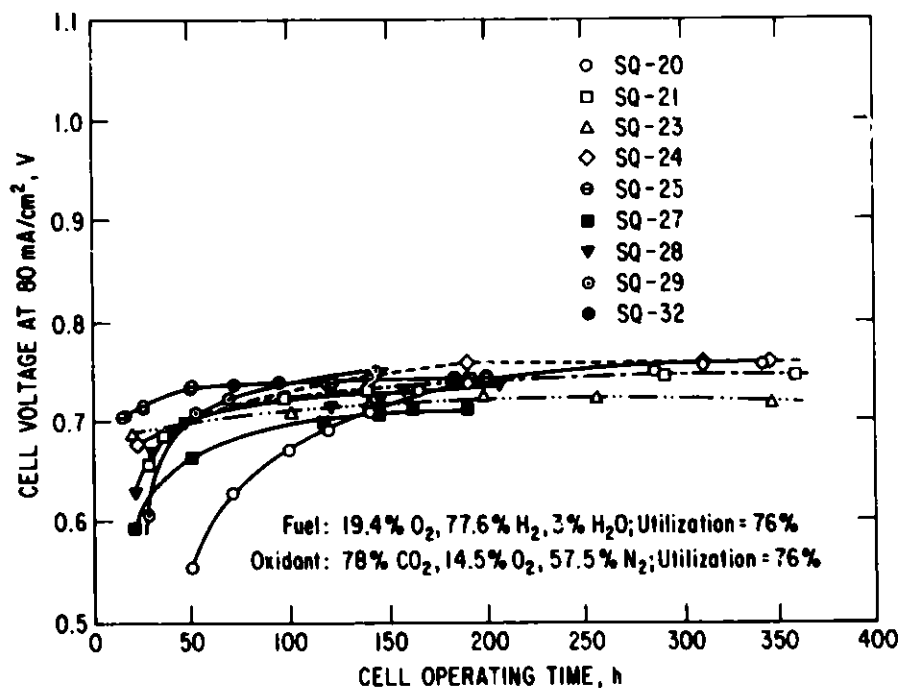

Fig. 2. Cell Voltage at 80 mA/cm^2 as a Function of Time

Figure 3 gives a plot of the constant-flow polarization data for cell SQ-32 as a function of time on test. The effective cell resistances were obtained from the slopes of the lines in the linear portion of the data (from the data points at 40- and 120-mA/cm^2 current density). The cell IR was found to be constant (within measurable limits) at 9 mΩ for the duration of the test.
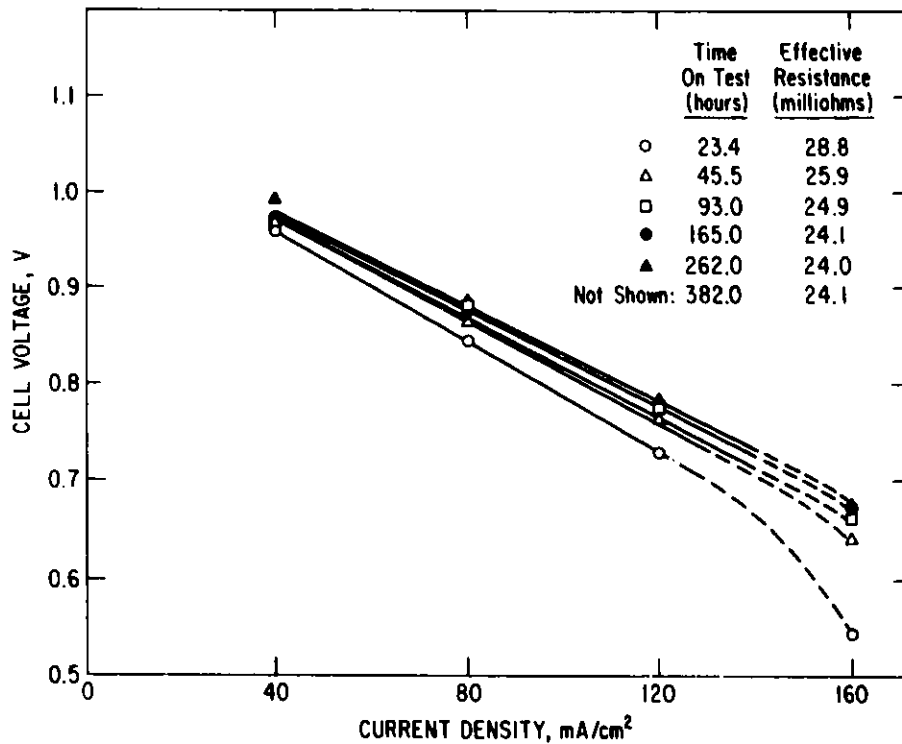
Fig. 3. Constant-Flow Polarization Data for SQ-32 as a
Function of Time (75% fuel utilization and 25%
oxidant utilization at 160 mA/cm^2; Cell IR =
9 mΩ)

Figure 4 is a plot of the effective cell resistance and ohmic resistances
obtained from current-inte interrupt measurements as a function of time. The dif-
ference between the two (i.e., upper curve minus lower curve) is attributed to
polarization losses (concentration and activation) occurring in the cell. The
relatively rapid early decrease in the polarization losses of cells SQ-25
and SQ-32 suggests that the incorporation of the nickel aluminate subcathode
layer may have a beneficial effect on the cathode-side polarization processes.

B. **Posttest Evaluations**

1. **Nickel Analysis and Cell LR-2 Results**
   (G. H. Kucera)

During this quarter, the posttest assessment of the components from
cell LR-2 was completed, and sampling techniques and methods to analyze for
nickel in posttest tiles were examined.

Examination of the components from cell LR-2, which operated for
2398 h and was used to study cathode potential relaxation, showed changes in
or on both current collectors. The posttest anode current collector was very
brittle and broke easily under a slight bending action. The cause of the
brittleness is not known; however, it may be the result of carburization or
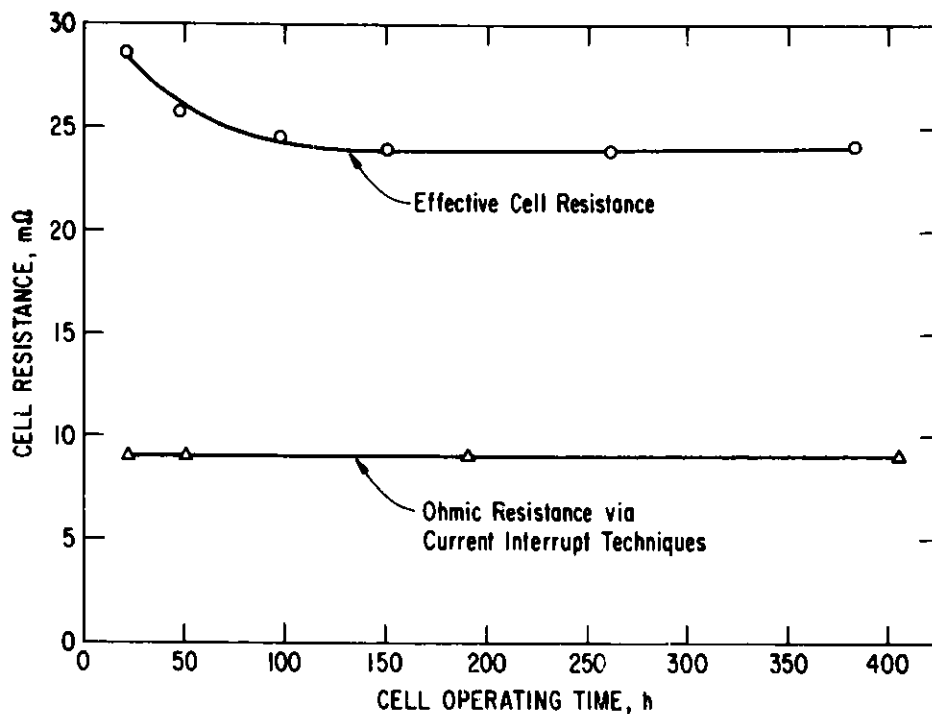
Fig. 4. Effective Cell and Ohmic Resistances for Cell SQ-32
        as a Function of Time

hydrogen embrittlement. A thin layer of yellow-green solid covered one sur-
face of the posttest cathode current collector on the side in contact with the
cell housing. X-ray diffraction analysis of the solid showed α-K_2CrO_4 as the
only phase. The tile lost about 4.7 cm^3 (~28%) of its carbonates, resulting
in a very dry tile. Only about 2.3 cm^3 carbonates were found in the other
components; additional electrolyte is known to have been wicked out by insu-
lation that accidently was in contact with one edge of the tile. The surface
area from $LiAlO_2$ in the posttest tile was 15 m^2/g. This represents a typical
surface area loss as seen in previous posttest tiles (ANL-82-40, p. 17).

        A number of analytical techniques were examined to determine the
most suitable methods for analyzing the nickel content and, perhaps, the
nickel species in some of our posttest tiles. These techniques include
energy-dispersive analysis of X-rays (EDS), energy-dispersive X-ray fluo-
rescence (EDXRF), electron microprobe, ion microprobe, and Auger electron
spectroscopy for chemical analyses (ESCA). The techniques EDS and EDXRF
differ in a number of ways. In EDS, direct electron excitation of the
specimen, which serves as the anode, causes X-rays to be emitted. The
energies of the emitted X-rays are measured directly. In EDXRF, primary
X-rays are produced by the electron excitation of a selected metal target.
These primary X-rays are then used to bombard the specimen, producing
secondary (fluorescent) X-rays. None of the above techniques gives a
quantitative assessment of the desired constituent in a specimen. However,
with the use of carefully prepared internal standards, a semiquantitative
(probably 5 to 10%) determination is possible. Because the sensitivity and

detection of a given constituent is dependent on the matrix, the standard must reflect the matrix in which the constituent resides. Furthermore, energy-dispersive and electron microprobe analyses do not distinguish between metallic nickel and certain nickel-bearing compounds in our tiles for two reasons: (1) certain low atomic-number elements are not detected--Z < 11 (sodium) with energy dispersive X-ray and Z < 6 (carbon) with the electron microprobe--and (2) chemical bonds cannot be discerned. In the first case, the ratio of nickel to other constituents in compounds containing a low atomic-number element such as lithium will be in error; and, in the second case, an intimate mixture of elements cannot be distinguished from a compound in which the constituents are present in the same ratio. Auger/ESCA and ion microprobe analysis can be used to determine the nickel species in a tile specimen. The former is the preferred method because the light atomic weight elements are matrix dependent in ion microprobe assessment.

In view of the above, two analytical approaches were chosen. In the first, a semiquantitative profiling of a piece of tile will be used to assess the distribution of the nickel and, when possible, to identify the nickel species. In the second, a quantitative chemical determination will be performed for the nickel.

In cell LR-2, a dark layer was observed on the tile located at the cathode-tile interface. To ascertain if this layer is to be considered part of the specimen submitted for chemical analysis or merely part of the cathode, a small portion was taken from the tile, washed free of carbonates, and submitted for X-ray diffraction analysis. The X-ray pattern showed γ- and β-$LiAlO_2$ as major phases, nickel metal and $LiNiO_2$ as medium phases, and NiO as a minor phase. In view of these X-ray results, it was concluded that this layer should be considered part of the tile specimen for analysis. A small specimen taken from a similar dark area, but located in a region about 1/3 of the way through the tile thickness, also showed $LiNiO_2$ as a phase, in addition to the expected γ- and β-$LiAlO_2$.

Specimens of tiles of four cells have been analyzed by the above approaches. A discussion of the migration and posttest location of nickel metal deposits is found in the next section. Table 4 is a summary of the quantity of nickel found in each of the tiles examined. As expected, the data show that the amount of nickel in the tile increases with cell operating time. Also shown are calulated transfer constants, which include the effects of diffusivity, tortuosity, and reduced area due to the $LiAlO_2$ particles. For this determination, the solubility of Ni^{2+} at the cathode was taken as 1.6×10^{-5} mole fraction (interpolated for 923 K from measurements made by General Electric[5]), and the nickel analyzed in the tile was all assumed to be deposited as metal. This constant has the units of diffusivity but is lower than the diffusion constant. Assuming that the nickel concentration in the tiles of cells SQ-23 and -26 is representative, we calculated that a typical (7.1 g) nickel cathode will be consumed in ~11,000-12,000 h under our cell operating conditions (1 atm air, 30% CO_2).

2. Posttest Cell Analysis
    (R. M. Arons)

The migration of corrosion products in a molten carbonate fuel cell has been an underlying but virtually unaddressed concern for some time. It

Table 4. Nickel Content in Tiles from Cells
SQ-23, -26, -27, and LR-2

Cell Number	Operating Time, h	Nickel, wt %	Nickel Transport Rate,[a] $mol/(cm^2 \cdot h)$	Transfer Constant, cm^2/s
SQ-23	459	0.92	1.4×10^{-7}	1.4×10^{-6}
SQ-26	198	0.28	0.99×10^{-7}	2.6×10^{-6}
SQ-29	380	0.81	1.5×10^{-7}	1.7×10^{-6}
LR-2	2398	2.75	0.75×10^{-7}	3.6×10^{-6}

[a]Based on the posttest tile weight and an effective tile area of 93 cm^2.

has been recognized that a number of cationic species having appreciable solubility in the electrolyte would possibly transport to regions of the cell reasonably distant from their source. For example, chromium might diffuse from stainless steel hardware or from the Ni-Cr anode through the electrolyte to the cathode, where Cr^{3+} could potentially poison the cathode's electrical conductivity. As reported earlier (ANL-81-68, p. 20), we found evidence of stainless steel corrosion products infused into the electrolyte from the cathode side of cell SQ-17. Iron, chromium, manganese, and nickel were detected deep within the electrolyte tile, using an SEM equipped with ELS. These elements plus cobalt and vanadium were found in another tile sample, using X-ray fluorescence (a more sensitive technique than EDS).

More recently, reports have come back from United Technologies Corp. that extensive metallic nickel precipitates have been found in the electrolyte of cells run for extended periods with high CO_2 partial pressure in the cathode gas[6]. As stated earlier, a mechanism exists whereby NiO dissolves to a very small extent from the cathode and diffuses as a cation to a region closer to the anode. When the cations encounter hydrogen diffusing from the anode, they are reduced to form metallic nickel.

Armed with the expectation that nickel metal may have been deposited in our tiles, we examined two used tiles for nickel deposits. A cross section of the first tile (denoted as sample A) was searched in an EDS equipped SEM and compared with a similar cross section of unused tile. The used ANL tiles generally have a grayish region near the cathode, which may vary in width but abruptly ends at some distance toward the anode; the tile appears white and unsullied for the remainder of the distance to the anode. Figure 5 shows a portion of an EDS spectrum from the gray region of sample A (shown with a solid line) superimposed on a spectrum from an unused tile (shown in dots). The spectrum from the virgin sample virtually mimics the used tile spectrum except for a notable peak at 7.5 keV, which coincides with the Kα lines for nickel. This peak demonstrates irrefutably that the used tile has picked up substantial

<4.02 keV   9.14 keV>
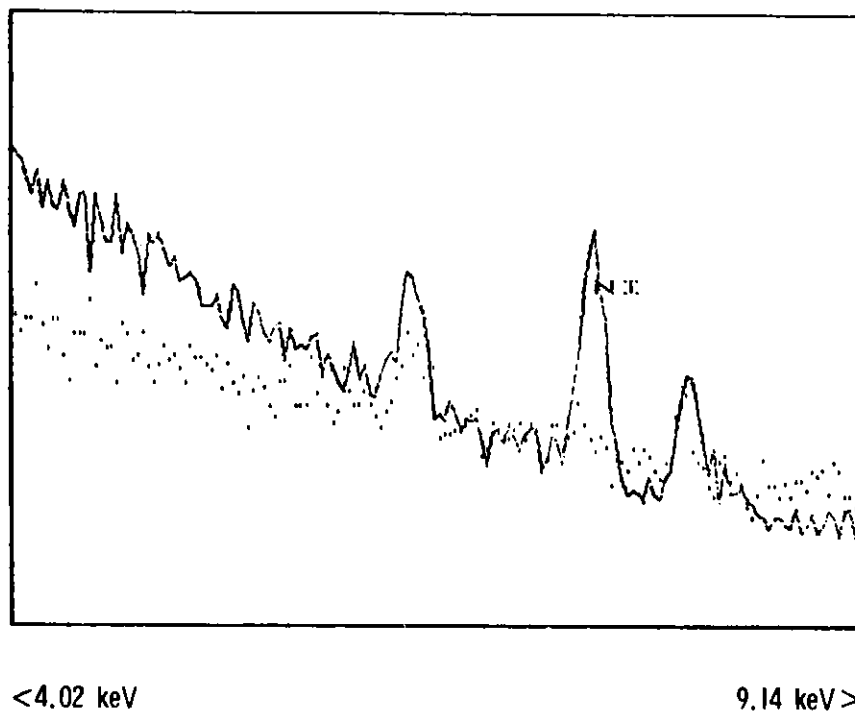
Fig. 5. Comparison of EDS Spectra of Used with
         Unused Tile. (The solid spectrum is
         that of the used tile.)

quantities of nickel. The height of the nickel peak was compared with the
potassium and aluminum peaks. In the virgin material, the ratio of peak
intensities for Al:K:Ni is 0.17:0.83:0.00, whereas in the used tile the
ratio is 0.28:0.66:0.07.

After X-ray intensity variations from atomic number, absorption,
and fluorescence yield (ZAF correction) are taken into account, the measured
atomic percent ratios of the elemental concentrations are 29% Al, 71% K, and
0% Ni in the virgin material and 45% Al, 52% K, and 3% Ni in the gray area of
the used tile. This method of analysis, of course, neglects lithium, oxygen,
carbon, and nitrogen because their atomic numbers are < 11. Although no pre-
cipitates of nickel were observed in this specimen, 3% nickel far exceeds the
solubility of nickel in the eutectic carbonate melt; and, therefore, the nickel
must be present as finely divided metallic particles or as an insoluble compound.

A second specimen (from cell LR-2) was similarly examined. In this
case, a band of small precipitates, roughly 5 μm in diameter, was found in
the tile parallel to the cathode, at a distance ranging from 0.3 to 0.6 mm
from the cathode. Figure 6 shows a micrograph of some of these precipitates
along with a nickel X-ray map. Quantitative EDS shows these precipitates to
be 99 wt % nickel and 1 wt % iron. Examination of a randomly chosen area
within the gray region of LR-2 gives the EDS spectrum shown in Fig. 7. In
addition to the nickel peaks at 7.5 and 8.3 keV, the tile gray area has
chromium peaks at 5.4 and 5.9 keV and iron peaks at 6.4 and 7.1 keV. This

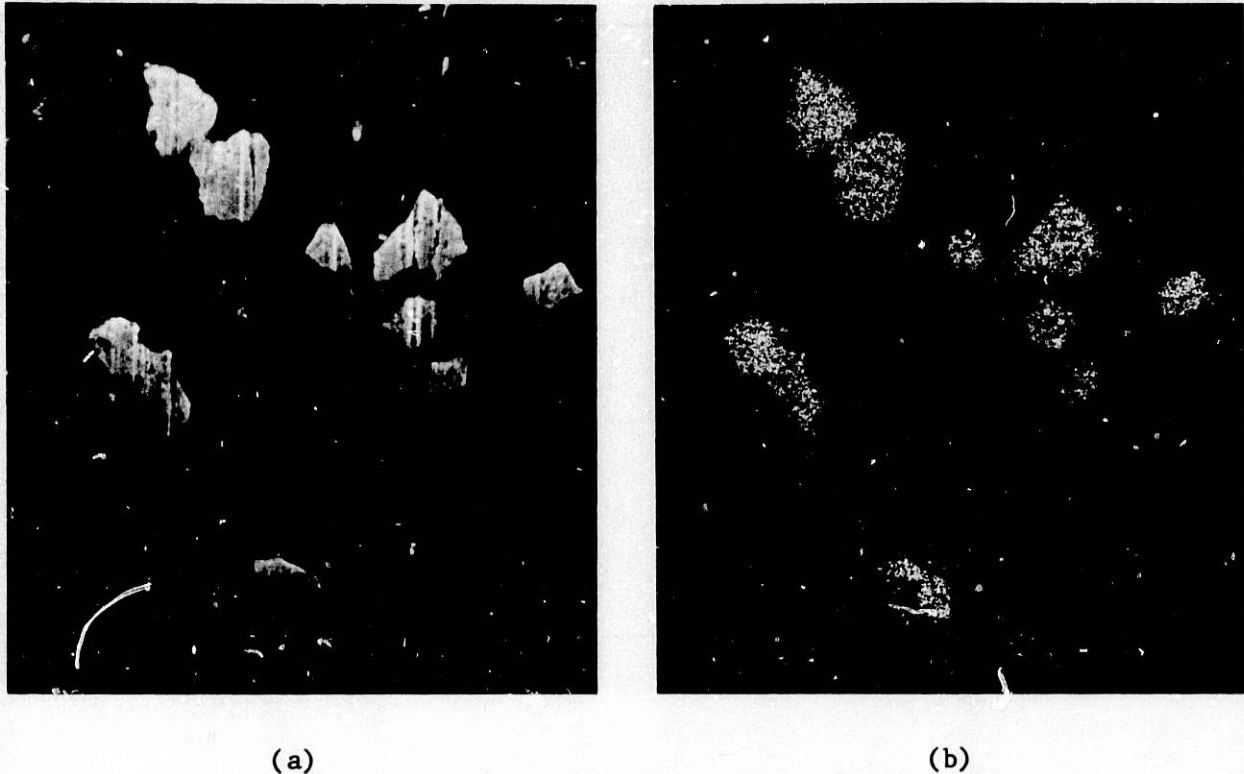(a)   (b)

Fig. 6.   SEM Micrographs of Precipitates Within Used MCFC Tile:
          (a) Secondary Electron Image and (b) Ni X-ray Map.

should be contrasted with the absence of a chromium peak and a very small iron peak in the virgin material. The iron peak in the virgin material arises from spurious signals in the SEM. An additional peak for both the used and unused tile shows up at about 1.8 keV and is attributable to silicon. Although silicon is an alloying element in stainless steels, it was probably introduced during specimen preparation with SiC abrasive paper.

A second band of precipitates was found in the LR-2 sample at about 0.25 mm from the cathode in the tile. These precipitates were clearly different in character from the more predominant precipitates just described. First, they were extremely difficult to find because they had so little contrast to the matrix under secondary electron imaging. Second, they ranged from 10 to 30 μm in diameter and were more irregularly shaped than the first precipitates. Finally, they appeared to be porous, whereas the original precipitates were dense. These observations suggest that the second type of precipitate is ceramic in character, and the first type is metallic.

The elements found in both tiles not attributable to tile preparation are contained in appreciable quantities in stainless steels. The source for all such elements except the nickel is believed to be the cathode cell housings and current collectors, which are fabricated from Type 316 stainless steel and showed extensive corrosion and oxidation upon cell disassembly. The nickel has a much more available source in the cathode.

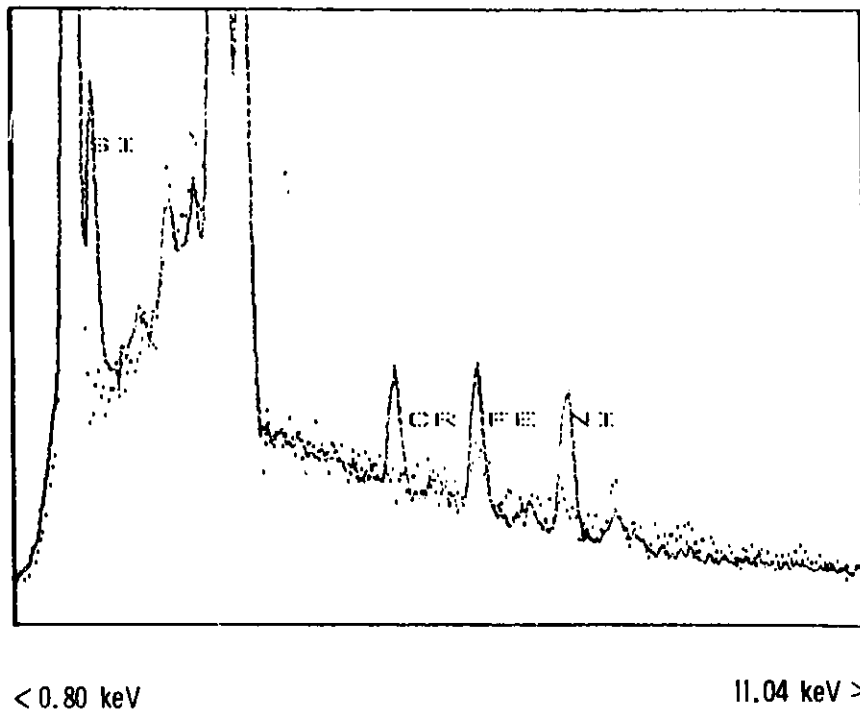< 0.80 keV   11.04 keV >

Fig. 7. Comparison of EDS Spectra of Used
         with Unused Tile. (The solid
         spectrum is that of the used tile.)

The LR-2 sample was further examined by electron microprobe, which
is an X-ray spectroscopy technique similar to EDS but which allows detection
of oxygen, nitrogen, and carbon. The microprobe was used to answer two
important questions. First, is there oxygen associated with the precipi-
tates, i.e., are they NiO, LiNiO$_2$, or some similar compound? Second, what
is the distribution of nickel in the tile? Careful microprobe examination
of the more predominant, first-observed precipitates was conducted by exciting
just the precipitate and the adjacent region. The precipitate was found to
be completely metallic, whereas the matrix around the precipitate was the normal
mixture of oxides and carbonates, as expected. (No information is available
regarding the lithium content of the precipitates.) In addition, the concen-
tration of nickel in the salt matrix was very low from the cathode to at least
the midpoint of the tile, and virtually all the nickel of consequence existed
as precipitates. The second type of precipitate, presumed to be ceramic, was
not examined in the microprobe.

As mentioned earlier, XRD analysis of the tile showed LiNiO$_2$. The
second type of nickel-containing precipitate, which was found using SEM/EDS,
is probably this LiNiO$_2$ compound, because no nickel-containing species other
than nickel and LiNiO$_2$ were identified with XRD. The finding of a compound
such as LiNiO$_2$ closer to the cathode (or farther from the H$_2$ source) than
the fully reduced nickel-metal precipitates is consistent with the migration
model.

Once certain features such as the composition of the metallic precipitates are identified, it is much simpler to examine additional samples via visible light microscopy and to correlate features observed with features known from electron optical techniques. The light microscope, although limited with respect to resolution and depth of field, has several advantages: one can observe visible light colors, obtain greater contrast between metallic and nonmetallic species, easily prepare samples, scan large areas more rapidly.

Using light microscopy, one can identify the nickel precipitate in a sample and then search for more precipitates in samples not examined with electron optics. Because metal precipitates are so distinctive in the light microscope, their number and distribution can be assessed more simply and with greater reliability, as compared to the electron optical techniques.

Specimens from four cells (LR-2, SQ-23, SQ-26, and SQ-29) were examined via light microscopy. Some micrographs were taken with cross polarizers, a technique found to yield the highest contrast among the unadulterated electrolyte matrix, the precipitates, and a corrosion-product-rich zone. Under polarized light, the region closest to the cathode showed a red-colored band that was adjacent to the cathode and extended into the tile. Some of the coloration appears to come from below a transparent surface. With polarized light, one can focus separately on surface features or on colored features at different focal distances. Under nonpolarized light, discontinuous coloration at the surface is only observed.

Each of the four specimens examined showed a red-colored zone, ranging from the cathode to the precipitates of nickel. This red region corresponds to a small concentration of iron and chromium, as identified by SEM/EDS. The red color is probably due to a defect or "color center" imposed on the ceramic tile materials by the Fe^{3+} or Cr^{3+}, much as Cr^{3+} colors corundum red in rubies. In general, the red zone stopped abruptly at the precipitates. The tile precipitates were found in a band anywhere from about 0.05 mm away from the tile/cathode interface to about 1/3 of the distance to the anode (0.7 mm in the case of cell LR-2). Beyond the precipitates, the tile looked unadulterated in all cells but LR-2. Examination of the LR-2 micrographs indicated that the red region had not traversed through the precipitate zone, but had skirted around islands of precipitates and spread out to a larger area once past them. Cell SQ-23 differed from the other three cells in that some nickel metal was found immediately adjacent to the cathode and ahead of the red band, i.e., nickel and NiO were evidently in direct contact (see Fig. 8).

Each of the four cells was operated under different conditions. An attempt will be made to correlate observed features with cell operation parameters in order to test consistency of the nickel and corrosion-product migration with current migration models.
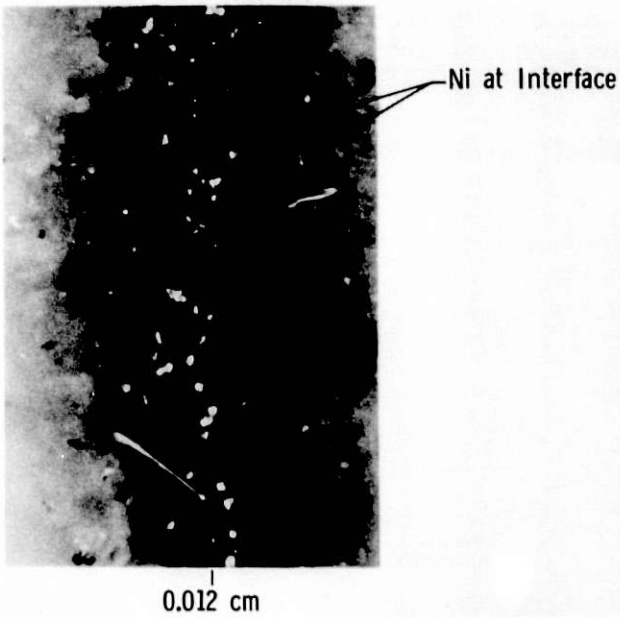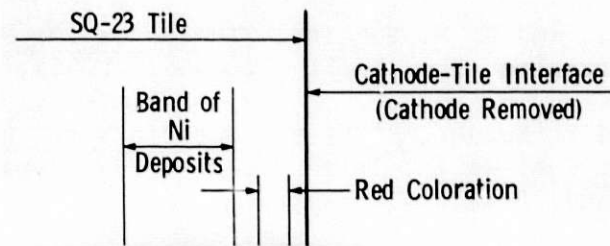
SQ-23 Tile

Cathode-Tile Interface
(Cathode Removed)

Band of
Ni
Deposits

Red Coloration

Ni at Interface

0.012 cm

Fig. 8.

Micrograph of Posttest
Electrolyte Tile from
Cell SQ-23

REFERENCES

1. C. F. Morel, J. Sci. Instrum. <u>43</u>, 647 (1966).

2. M. D. Ingram and G. J. Janz, The Thermodynamics of Corrosion in Molten Carbonates: Application of E/pCO$_2$ Diagrams, Electrochimica Acta 10, 783-792 (1965).

3. A. N. Webb, W. B. Mather, Jr., and R. M. Suggitt, Studies of the Molten Carbonate Fuel Cell, J. Electrochem. Soc. <u>12</u>(11), 1059-63 (1965).

4. T. Takahashi, H. Iwahara, and Y. Suzuki, Electrode Materials for High Temperature Solid Electrolyte Fuel Cells, Third International Symposium on Fuel Cells, June 16-20, 1969, Brussels, Belgium.

5. General Electric Co., Development of Molten Carbonate Fuel Cell Power Plant, Quarterly Technical Progress Report for August 1-October 31, 1981, Department of Energy Report DOE/ET/17019-7, pp. 42-62 (December 1981).

6. J. P. Ackerman, Argonne National Laboratory, private communication (1981).

Distribution for ANL-82-68

Internal:

J. P. Ackerman	T. D. Kaun	J. W. Sim
R. L. Breyne	M. Krumpelt	J. L. Smith
I.. Burris	G. H. Kucera	J. R. Stapay
F. A. Cafasso	N. Q. Minh	R. K. Steunenberg
T. D. Claar	F. C. Mrazek	E. H. VanDeventer
G. M. Cook	Z. Nagy	J. E. Young
J. T. Dusek	P. A. Nelson	S. A. Zwick
D. C. Fee	J. J. Picciolo	A. B. Krisciunas
P. A. Finn	R. D. Pierce (20)	ANL Patent Dept.
A. V. Fraioli	R. B. Poeppel	ANL Contract File
J. E. Harmon	J. J. Roberts	ANL Libraries (3)
A. A. Jonke	L. J. Ryan	TIS Files (6)

External:

DOE-TIC, for distribution per UC-93 (149)
Manager, Chicago Operations Office, DOE
R. J. Gariboldi, DOE-CH
Chemical Engineering Division Review Committee Members:
    C. B. Alcock, U. Toronto
    T. Cole, Jet Propulsion Lab.
    W. L. Worrell, U. Pennsylvania
Materials Science Division Review Committee:
    G. S. Ansell, Rensselaer Polytechnic Inst.
    A. Arrott, Simon Fraser U.
    A. L. Bement, Jr., TRW, Inc., Cleveland
    R. C. Dynes, Bell Labs., Murray Hill
    L. M. Falicov, U. California, Berkeley
    D. M. Ginsberg, U. Illinois, Urbana
    E. Kay, IBM San Jose Research Lab.
    M. E. Shank, Pratt & Whitney, East Hartford
    P. G. Shewmon, Ohio State U.
R. M. Arons, Celanese Research Co., Summit, N. J.
B. S. Baker, Energy Research Corp., Danbury, Conn.
T. R. Beck, Electrochemical Technology Corp., Seattle
E. Camara, Inst. Gas Technology, Chicago
T. W. Carter, U. S. Coast Guard, Washington
D. Chatterji, General Electric Co., Schenectady
J. Cuttica, Gas Research Inst., Chicago
L. M. Ferris, Oak Ridge National Lab.
A. P. Fickett, Electric Power Research Inst.
E. Gillis, Electric Power Research Inst.
J. Giner, Giner, Inc., Waltham, Mass.
F. Gmeindl, Morgantown Energy Technology Center
G. Hagey, Office of Coal Utilization, USDOE
J. W. Harrison, General Electric Co., Wilmington, Mass.
L. C. Headley, Morgantown Energy Technology Center
D. T. Hooie, Gas Research Inst., Chicago
D. Johnson, Northwestern U.
J. Kelly, Westinghouse R&D Center, Pittsburgh

K. Kinoshita, SRI International, Menlo Park
H. R. Kunz, United Technologies Corp., South Windsor, Conn.
A. R. Maret, Gas Research Inst., Chicago
N. Margalit, Combustion Engineering, Windsor
L. Marianowski, Inst. of Gas Technology, Chicago
H. Maru, Energy Research Corp., Danbury, Conn.
R. Matsumato, Ceramatech, Salt Lake City
A. P. Meyer, United Technologies Corp., South Windsor, Conn.
R. C. Osthoff, General Electric Co., Schenectady
J. R. Peterson, General Electric Co., Schenectady
C. A. Reiser, United Technologies Corp., South Windsor, Conn.
J. Searls, U. S. Bureau of Mines, Washington
R. Selman, Illinois Inst. of Technology
J. Sholes, Morgantown Energy Technology Center
P. Stonehart, Stonehart Associates, Inc., Madison, Conn.
G. Voelker, Office of Coal Utilization, USDOE
G. Wilemski, Physical Sciences Inc., Woburn, Mass.
K. Wray, Physical Sciences Inc., Woburn, Mass.
E. Yeager, Case Western Reserve U.